

# Probing the isospin structure and low-lying resonances in $\Lambda_c^+ \rightarrow n\bar{K}^0\pi^+$ decays

Meng-Yuan Li,<sup>1</sup> Guan-Ying Wang,<sup>2,\*</sup> Neng-Chang Wei,<sup>3,†</sup> De-Min Li,<sup>1,‡</sup> and En Wang<sup>1,§</sup>

<sup>1</sup>*School of Physics, Zhengzhou University, Zhengzhou 450001, China*

<sup>2</sup>*School of Physics and Electronics, Henan University, Kaifeng 475004, China*

<sup>3</sup>*School of Physics, Henan Normal University, Xinxiang 453007, China*

(Dated: February 16, 2026)

The Cabibbo-favored decay  $\Lambda_c^+ \rightarrow n\bar{K}^0\pi^+$  offers a unique window to explore unresolved puzzles in the low-energy baryon spectroscopy and the isospin dynamics of the  $\bar{K}N$  system. Recent experimental results present a, for now, contradiction: LHCb and Belle analyses of  $\Lambda_c^+ \rightarrow p\bar{K}^-\pi^+$  suggest the  $p\bar{K}^-$  ( $I = 0$ ) component dominates, while the BESIII hints at significant contributions from both isospin 0 and 1 in the  $n\bar{K}^0$  system of  $\Lambda_c^+ \rightarrow nK_S^0\pi^+$ . Furthermore, the measured branching fraction of  $\Lambda_c^+ \rightarrow nK_S^0\pi^+$  exceeds SU(3) symmetry predictions by a factor of 3-4, signaling strong contributions from low-lying resonances. In this work, we provide a theoretical analysis of  $\Lambda_c^+ \rightarrow n\bar{K}^0\pi^+$  within the coupled-channel chiral unitary approach, where the  $N(1535)$  and  $\Lambda(1670)$  can be dynamically generated. Our calculations show a narrow peak from  $N(1535)$  in the  $\pi^+n$  invariant mass spectrum and a distinct dip from  $\Lambda(1670)$  in the  $\bar{K}^0n$  spectrum. The dip structure is qualitatively consistent with the  $\Lambda(1670)$  manifestation in  $\bar{K}N \rightarrow \bar{K}N$  scattering, supporting its molecular interpretation. This study not only connects the experimental observations but also highlights  $\Lambda_c^+ \rightarrow n\bar{K}^0\pi^+$  as a crucial process to disentangle the nature of  $N(1535)$  and  $\Lambda(1670)$ . Future precise measurements of this decay channel by the BESIII, Belle II, LHCb, and the proposed Super Tau-Charm Factory are strongly encouraged.

## I. INTRODUCTION

Hadronic decays of charmed baryons serve as powerful laboratories for probing the structure of low-lying baryon resonances and the dynamics of final-state interactions [1–6]. Among these, the decay  $\Lambda_c^+ \rightarrow n\bar{K}^0\pi^+$  (or its neutral-kaon counterpart  $\Lambda_c^+ \rightarrow nK_S^0\pi^+$ ) has recently drawn significant attention due to intriguing experimental findings and its unique sensitivity to specific resonance contributions [7, 8].

The process  $\Lambda_c^+ \rightarrow nK_S^0\pi^+$  has been precisely measured by the BESIII Collaboration, yielding a branching fraction of  $(1.86 \pm 0.08 \pm 0.04) \times 10^{-2}$  [8]. This value is notably 3 to 4 times larger than theoretical predictions based on SU(3) flavor symmetry [9, 10], strongly suggesting the presence of significant resonant contributions beyond simple spectator diagrams. Since contributions from excited kaons are Cabibbo-suppressed in this decay, the dominant resonant enhancement likely stems from low-lying baryon states. Two prime candidates are the  $N(1535)$  ( $J^P = 1/2^-$ ) and the  $\Lambda(1670)$  ( $J^P = 1/2^-$ ), both of which couple strongly to channels involving strangeness.

However, the situation is complicated by an apparent discrepancy concerning the isospin composition of the  $\bar{K}N$  system in  $\Lambda_c^+$  decays. In the analysis of  $\Lambda_c^+ \rightarrow p\bar{K}^-\pi^+$ , both the LHCb [11] and Belle [12] collaborations found that the amplitude describing the  $p\bar{K}^-$  ( $I = 0$ ) pair is dominant, supported by the studies of Refs. [13, 14]. In contrast, BESIII's analysis of  $\Lambda_c^+ \rightarrow nK_S^0\pi^+$  suggests that the  $n\bar{K}^0$  system receives contributions from both isospin 0 and isospin 1 components, with comparable importance [8, 15]. This inconsistency calls

for a deeper theoretical investigation that connects these decay modes and clarifies the role of intermediate resonances, which can significantly alter the effective isospin projection observed in different final states.

The  $N(1535)$  resonance, the lowest-lying  $J^P = 1/2^-$  nucleon excitation, has long been a subject of debate regarding its internal structure [16, 17]. In the traditional quark model, it is described as a three-quark orbital excitation. However, its unexpectedly large couplings to  $\eta N$  and  $K\Lambda$  channels has motivated alternative interpretations, such as a significant pentaquark component  $[ud][us]\bar{s}$  [18–21] or a dynamically generated state from meson-baryon interactions within the chiral unitary approach [22–36]. Within the Hamiltonian effective field theory, the  $N(1535)$  resonance can be interpreted as a three-quark core generated from the meson-baryon scattering [37–39]. Recent studies using correlation functions and scattering lengths also explore its possible molecular nature [40, 41]. Thus,  $\Lambda_c^+ \rightarrow n\bar{K}^0\pi^+$ , where the  $\pi^+n$  spectrum provides a relatively clean environment for  $N(1535)$  (free from double Cabibbo-suppressed kaon excitations), is an ideal process to study this contested state.

The  $\Lambda(1670)$  resonance presents another fascinating puzzle due to its process-dependent line shapes. While it appears as a peak in the  $\eta\Lambda$  spectrum of  $\Lambda_c^+ \rightarrow \Lambda\pi^+\eta$  [42] and as a cusp near the  $\eta\Lambda$  threshold in the  $K^-p$  spectrum of  $\Lambda_c^+ \rightarrow p\bar{K}^-\pi^+$  [11, 12], it famously manifests as a dip in the  $\bar{K}N$  invariant mass distribution of the  $\bar{K}N \rightarrow \bar{K}N$  scattering process [43, 44]. On the other hand, the Crystal Ball Collaboration has measured the differential and total cross-section for the process  $K^-p \rightarrow \eta\Lambda$ , suggesting that the  $\Lambda(1670)$  is a three-quark state [45]. The study of the  $K^-p \rightarrow \pi^0\Lambda^0$  scattering process within the chiral quark model, supports the  $\Lambda(1670)$  as a traditional three-quark state [46]. In Ref. [47], the authors investigated the internal structure of  $\Lambda(1670)$  within the Hamiltonian effective field theory by combining lattice QCD simulations and experimental data, and prefer to describe  $\Lambda(1670)$  as a bare three-quark basis state that mixes with the  $\pi\Sigma$ ,  $\bar{K}N$ ,

\* [wangguanying@henu.edu.cn](mailto:wangguanying@henu.edu.cn)

† [weinengchang@htu.edu.cn](mailto:weinengchang@htu.edu.cn)

‡ [lidm@zzu.edu.cn](mailto:lidm@zzu.edu.cn)

§ [wangen@zzu.edu.cn](mailto:wangen@zzu.edu.cn)

$\eta\Lambda$ , and  $K\Xi$  meson-baryon channels. Thus, this transition from a peak to a cusp/dip across different production mechanisms highlights the sensitivity of its observable signature to interference with non-resonant backgrounds and the specific coupled channels involved. Theoretical interpretations of  $\Lambda(1670)$  also vary, with descriptions ranging from a conventional three-quark state [45–47] to a dynamically generated molecule from coupled-channel interactions like  $\bar{K}N$ ,  $\eta\Lambda$ , and  $\pi\Sigma$  [13, 14, 48–53]. The  $\bar{K}^0n$  spectrum in  $\Lambda_c^+ \rightarrow n\bar{K}^0\pi^+$  offers a new terrain to map the  $\Lambda(1670)$  line shape and test these interpretations.

In this work, we perform a theoretical analysis of the decay  $\Lambda_c^+ \rightarrow n\bar{K}^0\pi^+$  within the framework of the chiral unitary approach, where the  $N(1535)$  and  $\Lambda(1670)$  resonances are dynamically generated from  $S$ -wave pseudoscalar meson-octet baryon final-state interactions (FSI). Our primary goals are: (i) to provide theoretical predictions for the  $\pi^+n$  and  $\bar{K}^0n$  invariant mass distributions, highlighting the characteristic structures from  $N(1535)$  and  $\Lambda(1670)$ ; (ii) to discuss how these resonant contributions can be helpful to reconcile the observed experimental discrepancies in  $\bar{K}N$  isospin composition; and (iii) to emphasize the role of this decay channel as a unique probe for elucidating the nature of these two enigmatic low-lying resonances.

The paper is organized as follows. In Sec. II, we detail the theoretical framework, including the weak production mechanisms, the hadronization process, and the FSI leading to the dynamical generation of  $N(1535)$  and  $\Lambda(1670)$ . In Sec. III, we present and discuss our numerical results for the invariant mass distributions, the Dalitz plot, and the dependence on model parameters. A summary and outlook are given in Sec. IV.

## II. FORMALISM

In this section, we first present the theoretical formalism for the process  $\Lambda_c^+ \rightarrow n\bar{K}^0\pi^+$ . The decay process proceeds through three sequential steps: weak decay, hadronization, and final-state interaction. Then, we show the amplitude of the dynamically generated  $N(1535)$  in Sec. II A and that of the dynamically generated  $\Lambda(1670)$  in Sec. II B. Finally, we give the invariant mass distributions of the process  $\Lambda_c^+ \rightarrow n\bar{K}^0\pi^+$  in Sec. II C.

The quark-level diagram for the internal emission mechanism of  $\Lambda_c^+ \rightarrow n\bar{K}^0\pi^+$  is shown in Fig. 1, as done in Refs. [54, 55]. The process begins with the weak decay  $c \rightarrow sW^+$ , followed by  $W^+ \rightarrow u\bar{d}$ . Subsequently, the  $s$  quark and the  $\bar{d}$  quark from the  $W^+$  boson will hadronize into  $\bar{K}^0$ , while the  $u$  quark, the spectator  $ud$  diquark from the initial  $\Lambda_c^+$ , and a  $\bar{u}u + \bar{d}d + \bar{s}s$  pair created from the vacuum, hadronize into a meson-baryon pair. The flavor structure for the weak

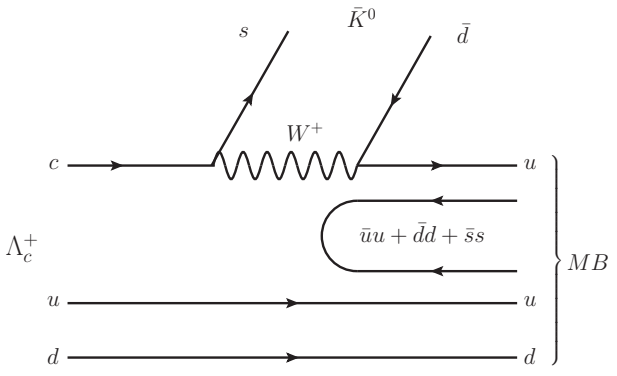


FIG. 1. Quark level diagram for the process  $\Lambda_c^+ \rightarrow \bar{K}^0 MB$  via the  $W^+$  internal emission.

decay and hadronization are given below,

$$\begin{aligned} \Lambda_c^+ &= \frac{1}{\sqrt{2}} c(u\bar{d} - d\bar{u}) \\ &\Rightarrow V_{cs} V_{ud} \frac{1}{\sqrt{2}} s\bar{d}u (\bar{u}u + \bar{d}d + \bar{s}s) (u\bar{d} - d\bar{u}) \\ &= V_{cs} V_{ud} \frac{1}{\sqrt{2}} \bar{K}^0 u (\bar{u}u + \bar{d}d + \bar{s}s) (u\bar{d} - d\bar{u}), \end{aligned} \quad (1)$$

where  $V_{cs}$  and  $V_{ud}$  denote the Cabibbo-Kobayashi-Maskawa (CKM) matrix elements for the quark transitions  $c \rightarrow s$  and  $u \rightarrow d$ , respectively. Within the  $SU(3)$  flavor symmetry, the quark and hadron degrees of freedom could be correlated by the ground pseudoscalar meson matrix  $M$  and the ground baryon octet matrix  $B$ , and the matrices  $M$  and  $B$  are expressed as [32, 56, 57],

$$M = \begin{pmatrix} u\bar{u} & u\bar{d} & u\bar{s} \\ d\bar{u} & d\bar{d} & d\bar{s} \\ s\bar{u} & s\bar{d} & s\bar{s} \end{pmatrix} = \begin{pmatrix} \frac{\eta}{\sqrt{3}} + \frac{\pi^0}{\sqrt{2}} + \frac{\eta'}{\sqrt{6}} & \pi^+ & K^+ \\ \pi^- & \frac{\eta}{\sqrt{3}} - \frac{\pi^0}{\sqrt{2}} + \frac{\eta'}{\sqrt{6}} & K^0 \\ K^- & \bar{K}^0 & -\frac{\eta}{\sqrt{3}} + \frac{\sqrt{6}\eta'}{3} \end{pmatrix}, \quad (2)$$

$$B = \frac{1}{\sqrt{2}} \begin{pmatrix} u(ds - sd) & u(su - us) & u(u\bar{d} - d\bar{u}) \\ d(ds - sd) & d(su - us) & d(u\bar{d} - d\bar{u}) \\ s(ds - sd) & s(su - us) & s(u\bar{d} - d\bar{u}) \end{pmatrix} = \begin{pmatrix} \frac{\Sigma^0}{\sqrt{2}} + \frac{\Lambda}{\sqrt{6}} & \Sigma^+ & p \\ \Sigma^- & -\frac{\Sigma^0}{\sqrt{2}} + \frac{\Lambda}{\sqrt{6}} & n \\ \Xi^- & \Xi^0 & -\frac{2\Lambda}{\sqrt{6}} \end{pmatrix}, \quad (3)$$

where we adopt the  $\eta$ - $\eta'$  standard mixing [58]. Given that the  $\eta'$  has a large mass and is typically omitted in chiral Lagrangians [59], we neglect the meson-baryon pair involving

the  $\eta'$ . Then, the available final  $|MB\rangle$  pairs are written as,

$$\begin{aligned} |MB\rangle &= \frac{1}{\sqrt{2}}|u(\bar{u}u + \bar{d}d + \bar{s}s)(ud - du)\rangle \\ &= \sum_{i=1}^3 |M_{1i}B_{i3}\rangle \\ &= \frac{1}{\sqrt{2}}|\pi^0 p\rangle + \frac{1}{\sqrt{3}}|\eta p\rangle + |\pi^+ n\rangle - \sqrt{\frac{2}{3}}|K^+ \Lambda\rangle, \end{aligned} \quad (4)$$

where  $i = 1, 2, 3$  corresponds to the  $u$ ,  $d$ , and  $s$  quarks, respectively. Thus, the total amplitude for the internal emission mechanism contributing to  $\Lambda_c^+ \rightarrow \bar{K}^0 X$ , where  $X$  later undergoes FSI, is,

$$\mathcal{M}^{\text{in}} = V_p V_{cs} V_{ud} \bar{K}^0 \left( \frac{1}{\sqrt{2}}\pi^0 p + \frac{1}{\sqrt{3}}\eta p + \pi^+ n - \sqrt{\frac{2}{3}}K^+ \Lambda \right), \quad (5)$$

where  $V_p$  is a constant factor encoding the weak transition strength.

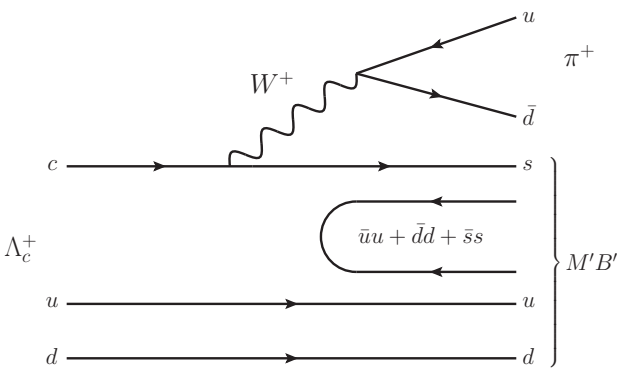


FIG. 2. Quark level diagram for the process  $\Lambda_c^+ \rightarrow \pi^+ M'B'$  via the  $W^+$  external emission.

Subsequently, we present the quark-level diagram for the external emission mechanism of the decay  $\Lambda_c^+ \rightarrow n\bar{K}^0\pi^+$  in Fig. 2. In the first step, the charm quark of initial  $\Lambda_c^+$  decays into an strange quark and a  $u\bar{d}$  pair by the weak interaction, then the  $u\bar{d}$  quark pair hadronizes into a  $\pi^+$ . Meanwhile, the  $sud$  cluster hadronizes with the antiquark-quark pair  $\bar{u}u + \bar{d}d + \bar{s}s$  created from the vacuum, and we could obtain,

$$\begin{aligned} \Lambda_c^+ &= V_{cs} V_{ud} \frac{1}{\sqrt{2}} c (ud - du) \\ &\Rightarrow V_{cs} V_{ud} \frac{1}{\sqrt{2}} u \bar{d} s (\bar{u}u + \bar{d}d + \bar{s}s) (ud - du) \\ &= V_{cs} V_{ud} \frac{1}{\sqrt{2}} \pi^+ s (\bar{u}u + \bar{d}d + \bar{s}s) (ud - du). \end{aligned} \quad (6)$$

The resulting meson-baryon state  $|M'B'\rangle$  in Fig. 2 can be writ-

ten as,

$$\begin{aligned} |M'B'\rangle &= \frac{1}{\sqrt{2}}|s(\bar{u}u + \bar{d}d + \bar{s}s)(ud - du)\rangle \\ &= \sum_{i=1}^3 |M'_{3i}B'_{i3}\rangle \\ &= |K^- p\rangle + |\bar{K}^0 n\rangle + \frac{\sqrt{2}}{3}|\eta \Lambda\rangle. \end{aligned} \quad (7)$$

The external emission amplitude is therefore,

$$\mathcal{M}^{\text{ex}} = CV_p V_{cs} V_{ud} \pi^+ \left( K^- p + \bar{K}^0 n + \frac{\sqrt{2}}{3} \eta \Lambda \right), \quad (8)$$

where the color factor  $C$  accounts for the relative weight of the external vs. internal emission diagrams. Both mechanisms are Cabibbo-favored and of the same order.

### A. Dynamical Generation of $N(1535)$

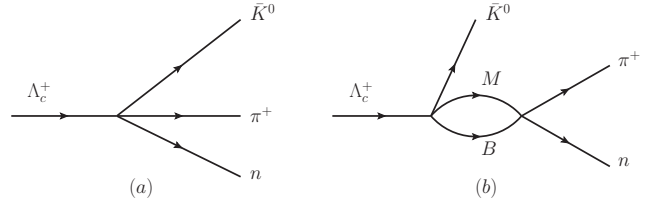


FIG. 3. The diagrams for the Tree-level (a) and the  $MB$  rescattering (b) of the  $\Lambda_c^+ \rightarrow n\bar{K}^0\pi^+$  decay.

As depicted in Fig. 3(a), the final state  $n\bar{K}^0\pi^+$  could be generated directly. Furthermore, this final state may also arise from the rescattering of intermediate meson-baryon pair in  $S$ -wave, as illustrated in Fig. 3(b), which could dynamically generate the  $N(1535)$ . As we discussed in the introduction, the  $N(1535)$  resonance is dynamically generated from the  $S$ -wave interaction of pseudoscalar mesons with octet baryons in the strangeness  $S = 0$ , isospin  $I = 1/2$  sector. We consider the coupled channels:  $\pi^0 p$ ,  $\pi^+ n$ ,  $\eta p$ ,  $K^+ \Lambda$ ,  $K^0 \Sigma^+$ , and  $K^+ \Sigma^0$ . Based on the final-state components given in Eqs. (5) and (8), the decay amplitude corresponding to the dynamically generated  $N(1535)$  resonance could be expressed as,

$$\begin{aligned} \mathcal{T}^{N(1535)} &= V_p \left( h_{\pi^+ n} + h_{\pi^0 p} \tilde{G}_{\pi^0 p}(M_{\pi^+ n}) t_{\pi^0 p \rightarrow \pi^+ n}(M_{\pi^+ n}) \right. \\ &\quad + h_{\eta p} \tilde{G}_{\eta p}(M_{\pi^+ n}) t_{\eta p \rightarrow \pi^+ n}(M_{\pi^+ n}) \\ &\quad + h_{\pi^+ n} \tilde{G}_{\pi^+ n}(M_{\pi^+ n}) t_{\pi^+ n \rightarrow \pi^+ n}(M_{\pi^+ n}) \\ &\quad \left. + h_{K^+ \Lambda} \tilde{G}_{K^+ \Lambda}(M_{\pi^+ n}) t_{K^+ \Lambda \rightarrow \pi^+ n}(M_{\pi^+ n}) \right) \\ &\quad + CV_p \left( h_{\bar{K}^0 n} \tilde{G}_{\pi^+ n}(M_{\pi^+ n}) t_{\pi^+ n \rightarrow \pi^+ n}(M_{\pi^+ n}) \right) \end{aligned} \quad (9)$$

where the coefficients  $h_{MB}$  represent the weights of the respective coupling channels in the hadronization process, and we can

obtain from Eqs. (5) and (8),

$$h_{\pi^0 p} = \frac{1}{\sqrt{2}}, \quad h_{\eta p} = \frac{1}{\sqrt{3}}, \quad h_{\pi^+ n} = 1, \quad h_{K^+ \Lambda} = -\sqrt{\frac{2}{3}}, \quad h_{\bar{K}^0 n} = 1. \quad (10)$$

The coupled channels transition amplitude of  $t_{MB \rightarrow \pi^+ n}$  in Eq. (9), which can be obtained by solving the Bethe-Salpeter equation

$$T = [1 - VG]^{-1} V, \quad (11)$$

where  $G$  is the meson-baryon loop function, and the interaction kernel  $V$  is taken from the leading order of the chiral Lagrangian, while we take it from Ref. [28]

$$V_{ij} = -C_{ij} \frac{1}{4f_i f_j} (2\sqrt{s} - M_i - M_j) \times \left( \frac{M_i + E_i}{2M_i} \right)^{1/2} \left( \frac{M_j + E_j}{2M_j} \right)^{1/2}, \quad (12)$$

where  $M_{i(j)}$  and  $E_{i(j)}$  are the mass and energy of the baryon in the  $i(j)$  channel, with  $E_i = (s + M_i^2 - m_i^2)/2\sqrt{s}$ . The coefficients  $C_{ij}$  are taken from Table I, with the pseudoscalar decay constants  $f_{i(j)}$  as follows,

$$f_\pi = 93 \text{ MeV}, \quad f_K = 1.22 f_\pi, \quad f_\eta = 1.3 f_\pi. \quad (13)$$

The meson-baryon system loop function  $G$  in Eq. (11) is given by [26],

$$G_i = i \int \frac{d^4 q}{(2\pi)^4} \frac{2M_i}{(P - q)^2 - M_i^2 + i\epsilon} \frac{1}{q^2 - m_i^2 + i\epsilon}, \quad (14)$$

where  $M_i(m_i)$  is the baryon(meson) mass for the  $i$ -th coupled channel.  $P$  is the four-momentum of the meson-baryon system, and  $q$  is the meson four-momentum in the center-of-mass frame. The loop function  $G_i$  in Eq. (14) is divergent, and we typically adopt either the three-momentum cutoff method or the dimensional regularization method for its renormalization. In this work, we employ dimensional regularization method, and the corresponding meson-baryon loop function  $G_{MB}$  can be written as [28, 54],

$$G(MB) = \frac{2M_B}{16\pi^2} \left\{ a_{MB}(\mu) + \ln \frac{M_B^2}{\mu^2} + \frac{m_M^2 - M_B^2 + s}{2s} \ln \frac{m_M^2}{M_B^2} + \frac{q_{MB}}{\sqrt{s}} \left[ \ln(s - (M_B^2 - m_M^2)) + 2q_{MB}\sqrt{s} \right] + \ln(s + (M_B^2 - m_M^2)) + 2q_{MB}\sqrt{s} - \ln(-s + (M_B^2 - m_M^2)) + 2q_{MB}\sqrt{s} - \ln(-s - (M_B^2 - m_M^2)) + 2q_{MB}\sqrt{s} \right\}, \quad (15)$$

where  $\sqrt{s}$  is the invariant mass of the  $MB$  pair,  $m_M$  and  $M_B$  are the meson and baryon masses for the coupled channels, respectively. The  $q_{MB}$  is the meson momentum in the meson-baryon center-of-mass frame, with  $q_{MB} =$

$\lambda^{1/2}(s, m_M^2, M_B^2)/2\sqrt{s}$ . The regularization scale  $\mu$  and the subtraction constant  $a_{MB}(\mu)$  are determined by fitting to the experimental data. Following Ref. [26], we take  $\mu = 1200$  MeV for each channel and the values for the subtraction constants are as follows:

$$a_{K^0 \Sigma^+}(\mu) = -2.8, \quad a_{K^+ \Sigma^0}(\mu) = -2.8, \quad a_{K^+ \Lambda}(\mu) = 1.6, \\ a_{\pi^+ n}(\mu) = 2.0, \quad a_{\pi^0 p}(\mu) = 2.0, \quad a_{\eta p}(\mu) = 0.2. \quad (16)$$

As done in Refs. [28, 29], the meson-baryon loop function  $\tilde{G}$  in Eq. (9) employs the cutoff method, rather than the dimensional regularization, and we take a cutoff momentum of  $|\tilde{q}_{\max}| = 1300$  MeV in our calculation. The form of  $\tilde{G}$  is given by,

$$\tilde{G}_i(M_{\pi^+ n}) = \int \frac{d^3 q}{(2\pi)^3} \frac{M_i}{2\omega_i(q)E_i(q)} \times \frac{1}{M_{\pi^+ n} - \omega_i(q) - E_i(q) + i\epsilon}, \quad (17)$$

where  $M_i$ ,  $E_i$ , and  $\omega_i$  are the baryon mass, baryon energy and meson energy of the  $i$ -th channel.

TABLE I. Coefficients  $C_{ij}$  for the  $S$ -wave meson-baryon ( $MB$ ) scattering [60].

	$K^0 \Sigma^+$	$K^+ \Sigma^0$	$K^+ \Lambda$	$\pi^+ n$	$\pi^0 p$	$\eta p$
$K^0 \Sigma^+$	1	$\sqrt{2}$	0	0	$1/\sqrt{2}$	$-\sqrt{3}/2$
$K^+ \Sigma^0$		0	0	$1/\sqrt{2}$	$-1/2$	$-\sqrt{3}/2$
$K^+ \Lambda$			0	$-\sqrt{3}/2$	$-\sqrt{3}/2$	$-3/2$
$\pi^+ n$				1	$\sqrt{2}$	0
$\pi^0 p$					0	0
$\eta p$						0

## B. Dynamical Generation of $\Lambda(1670)$

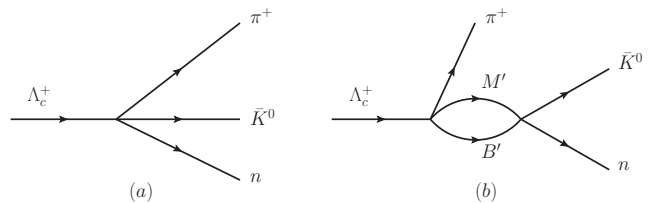


FIG. 4. The diagrams for the Tree-level (a) and the  $M'B'$  rescattering (b) of the  $\Lambda_c^+ \rightarrow n \bar{K}^0 \pi^+$  decay.

In this subsection, we investigate the  $\bar{K}^0 n$  final-state interaction which dynamically generates the  $\Lambda(1670)$  resonance as shown in Fig. 4. The mechanism includes both tree-level and rescattering contributions to the decay. Based on Eqs. (5)

and (8), the decay amplitude for the  $\Lambda(1670)$  contribution to  $\Lambda_c^+ \rightarrow n\bar{K}^0\pi^+$  could be expressed as

$$\begin{aligned} \mathcal{T}^{\Lambda(1670)} &= CV_p \left( h_{\bar{K}^0n} + h_{K^-p} G_{K^-p}(M_{\bar{K}^0n}) t_{K^-p \rightarrow \bar{K}^0n}(M_{\bar{K}^0n}) \right. \\ &\quad + h_{\bar{K}^0n} G_{\bar{K}^0n}(M_{\bar{K}^0n}) t_{\bar{K}^0n \rightarrow \bar{K}^0n}(M_{\bar{K}^0n}) \\ &\quad \left. + h_{\eta\Lambda} G_{\eta\Lambda}(M_{\bar{K}^0n}) t_{\eta\Lambda \rightarrow \bar{K}^0n}(M_{\bar{K}^0n}) \right) \\ &\quad + V_p \left( h_{\pi^+n} G_{\bar{K}^0n}(M_{\bar{K}^0n}) t_{\bar{K}^0n \rightarrow \bar{K}^0n}(M_{\bar{K}^0n}) \right) \quad (18) \end{aligned}$$

with  $h_{K^-p} = 1$  and  $h_{\eta\Lambda} = \sqrt{2}/3$ . The meson-baryon loop function  $G$  follows the same form as Eq. (15), while the meson-baryon transition amplitude  $t_{M'B' \rightarrow \bar{K}^0n}$  is likewise obtained through the Bethe-Salpeter equation as Eq. (11). The  $\Lambda(1670)$  resonance is dynamically generated in the strangeness  $S = -1$ , isospin  $I = 0$  sector. We consider ten coupled channels:  $K^-p$ ,  $\bar{K}^0n$ ,  $\pi^0\Lambda$ ,  $\pi^0\Sigma^0$ ,  $\eta\Lambda$ ,  $\eta\Sigma^0$ ,  $\pi^+\Sigma^-$ ,  $\pi^-\Sigma^+$ ,  $K^+\Xi^-$ , and  $K^0\Xi^0$ . Here, we take  $\mu = 630$  MeV, and the subtraction constants for each coupled channel are  $a_{\bar{K}N} = -1.84$ ,  $a_{\pi\Sigma} = -2.00$ ,  $a_{\pi\Lambda} = -1.83$ ,  $a_{\eta\Lambda} = -2.25$ ,  $a_{\eta\Sigma} = -2.38$ , and  $a_{K\Xi} = -2.52$ , taken from Ref. [44].

The transition potentials  $V'_{ij}$  between the ten channels are given by [44],

$$\begin{aligned} V'_{ij} &= -C'_{ij} \frac{1}{4f^2} (2\sqrt{s} - M_i - M_j) \\ &\quad \times \left( \frac{M_i + E_i}{2M_i} \right)^{1/2} \left( \frac{M_j + E_j}{2M_j} \right)^{1/2}, \quad (19) \end{aligned}$$

where  $f = 1.15f_\pi$ , and the coefficients  $C'_{ij}$  are given in Table I of Ref. [22].

It should be pointed out that the pole position of  $\Lambda(1670)$  is highly sensitive to the parameter  $a_{K\Xi}$ , while it is only moderately sensitive to the subtraction constants  $a_{\bar{K}N}$ ,  $a_{\pi\Sigma}$ , and  $a_{\eta\Lambda}$ . In Refs. [13, 49, 52], the authors determine  $a_{K\Xi}$  by fitting to the experimental data. Since no experimental data are provided for the decay  $\Lambda_c^+ \rightarrow n\bar{K}^0\pi^+$ , we adopt  $a_{K\Xi} = -2.776$  from Ref. [13]. Future measurements of  $\Lambda_c^+ \rightarrow n\bar{K}^0\pi^+$  could help to constrain this parameter.

### C. Invariant Mass Distributions

Based on the theoretical formalisms mentioned above, one can write down the double differential width of the process  $\Lambda_c^+ \rightarrow n\bar{K}^0\pi^+$  as

$$\frac{d^2\Gamma}{dM_{\pi^+n} dM_{\bar{K}^0n}} = \frac{1}{(2\pi)^3} \frac{M_n}{2M_{\Lambda_c^+}^2} |\mathcal{T}|^2 M_{\pi^+n} M_{\bar{K}^0n}, \quad (20)$$

where  $M_{\pi^+n}$  and  $M_{\bar{K}^0n}$  are the invariant masses of the indicated pairs, respectively.  $\mathcal{T}$  is the total decay amplitude for the decay  $\Lambda_c^+ \rightarrow n\bar{K}^0\pi^+$ ,

$$\mathcal{T} = \mathcal{T}^{N(1535)} + \mathcal{T}^{\Lambda(1670)} \times e^{i\phi}, \quad (21)$$

including a possible relative phase angle  $\phi$ .

One could easily obtain the single differential decay widths  $d\Gamma/dM_{\pi^+n}$  and  $d\Gamma/dM_{\bar{K}^0n}$  by integrating over the other invariant mass within its kinematically allowed range. For a fixed  $M_{12}$ , the corresponding range for the  $M_{23}$  is [61],

$$\begin{aligned} (M_{23})_{\min} &= \sqrt{\left( E_2^* + E_3^* \right)^2 - \left( \sqrt{E_2^{*2} - m_2^2} + \sqrt{E_3^{*2} - m_3^2} \right)^2}, \\ (M_{23})_{\max} &= \sqrt{\left( E_2^* + E_3^* \right)^2 - \left( \sqrt{E_2^{*2} - m_2^2} - \sqrt{E_3^{*2} - m_3^2} \right)^2}, \end{aligned} \quad (22)$$

where  $E_2^*$  and  $E_3^*$  are the energies of particles 2 and 3 in the rest frame of  $M_{12}$ , respectively,

$$\begin{aligned} E_2^* &= \frac{M_{12}^2 - m_1^2 + m_2^2}{2M_{12}}, \\ E_3^* &= \frac{M_{\Lambda_c^+}^2 - M_{12}^2 - m_3^2}{2M_{12}}, \end{aligned} \quad (23)$$

where  $m_1$ ,  $m_2$ , and  $m_3$  represent the masses of particles 1, 2, and 3, respectively. The masses and widths of the relevant particles are taken from the Review of Particle Physics (RPP) [61]. Since absolute experimental distributions are not yet available, we set the overall normalization  $V_P = 1$  and the color factor  $C = 3$  as a reference. Our predictions focus on the line shapes, which are independent of this overall normalization.

## III. RESULTS AND DISCUSSION

### A. Transition Amplitudes and Resonance Signals

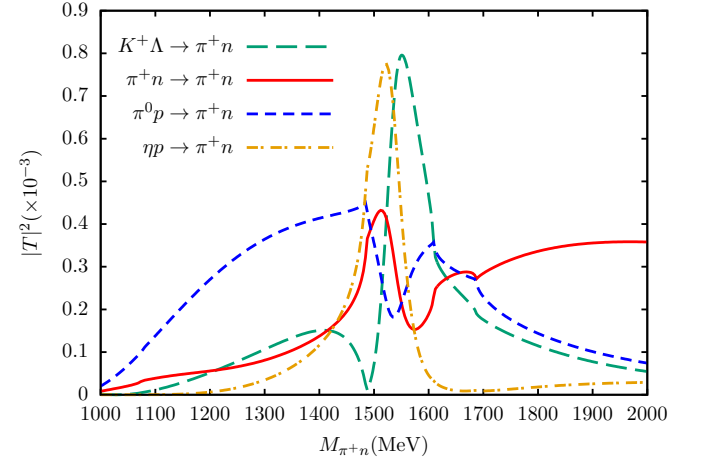


FIG. 5. Modulus squared of the transition amplitudes  $t_{MB \rightarrow \pi^+n}$  in S-wave.

We first examine the transition amplitudes  $t_{MB \rightarrow \pi^+n}$  and  $t_{M'B' \rightarrow \bar{K}^0n}$  that dynamically generate the resonances. Figure 5 shows  $|t_{MB \rightarrow \pi^+n}|^2$  for several initial channels. The green-dashed curve denotes the modulus squared of the transition

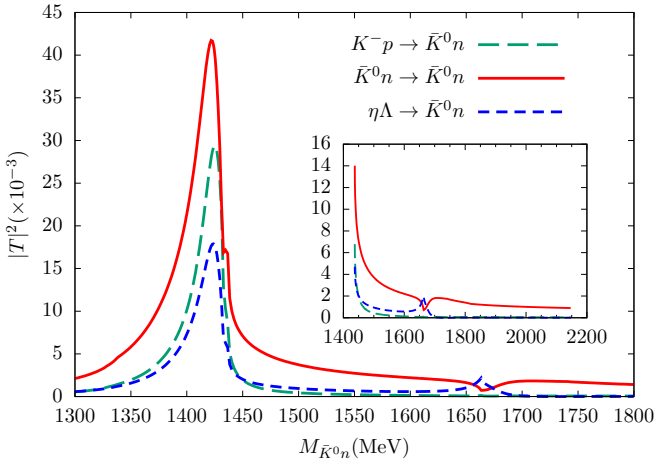


FIG. 6. Modulus squared of the transition amplitudes  $t_{M'B' \rightarrow \bar{K}^0 n}$  in S-wave. The inner sub-figures show the results within the  $\bar{K}^0 n$  phase space.

amplitude  $t_{K^+\Lambda \rightarrow \pi^+ n}$ , the red-solid curve denotes the modulus squared of the transition amplitude  $t_{\pi^+ n \rightarrow \pi^+ n}$ , the blue-dashed curve denotes the modulus squared of the transition amplitude  $t_{\pi^+ p \rightarrow \pi^+ n}$ , and the yellow-dashed-dotted curve denotes the modulus squared of the transition amplitude  $t_{\eta p \rightarrow \pi^+ n}$ . A clear peak around 1500 MeV is visible, corresponding to the  $N(1535)$  resonance. The  $\pi^+ n \rightarrow \pi^+ n$  amplitude (red solid curve) shows the strong signal, as expected for the dominant decay channel.

Figure 6 displays  $|t_{M'B' \rightarrow \bar{K}^0 n}|^2$ . The green-dashed curve denotes the modulus squared of the transition amplitude  $t_{K^-p \rightarrow \bar{K}^0 n}$ , the red-solid curve denotes the modulus squared of the transition amplitude  $t_{\bar{K}^0 n \rightarrow \bar{K}^0 n}$ , and the blue-dashed curve denotes the modulus squared of the transition amplitude  $t_{\eta\Lambda \rightarrow \bar{K}^0 n}$ . A prominent peak around 1420 MeV (the  $\Lambda(1405)$ ) and a clear dip structure around 1670 MeV (the  $\Lambda(1670)$ ) are seen in the  $\bar{K}^0 n \rightarrow \bar{K}^0 n$  amplitude (red solid curve). The  $\Lambda(1405)$  lies below the  $\bar{K}^0 n$  threshold ( $\sim 1430$  MeV) and thus contribute to the threshold of the  $\bar{K}^0 n$  spectrum in this decay. The inset focuses on the physical region, highlighting the  $\Lambda(1670)$  dip. The appearance of a dip (instead of a peak) is a characteristic prediction of the chiral unitary approach for  $\Lambda(1670)$  in the  $\bar{K}N$  channel and is consistent with its manifestation in  $\bar{K}N \rightarrow \bar{K}N$  scattering data [43, 44]. This occurs due to a strong destructive interference between the resonant amplitude and the non-resonant background, driven by the phase motion of the  $\Lambda(1670)$  pole located near the  $\eta\Lambda$  threshold.

## B. Invariant Mass Distributions and Dalitz Plot for $\Lambda_c^+ \rightarrow \bar{K}^0 \pi^+ n$

Our main results for the  $\pi^+ n$  and  $\bar{K}^0 n$  invariant mass distributions are presented in Fig. 7. The individual contributions from  $N(1535)$  (blue dash-dotted) and  $\Lambda(1670)$  (red dotted), as well as their coherent sum with  $\phi = 0$  (black solid), are shown.

In the  $\pi^+ n$  distribution (Fig. 7(a)), a pronounced narrow

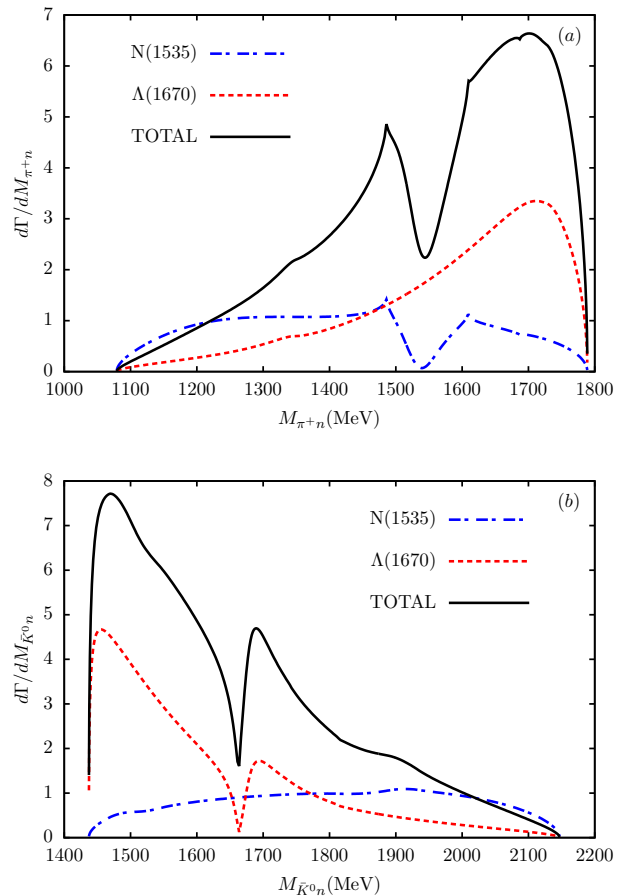


FIG. 7.  $\pi^+ n$  (a) and  $\bar{K}^0 n$  (b) invariant mass distributions of the process  $\Lambda_c^+ \rightarrow n\bar{K}^0\pi^+$ .

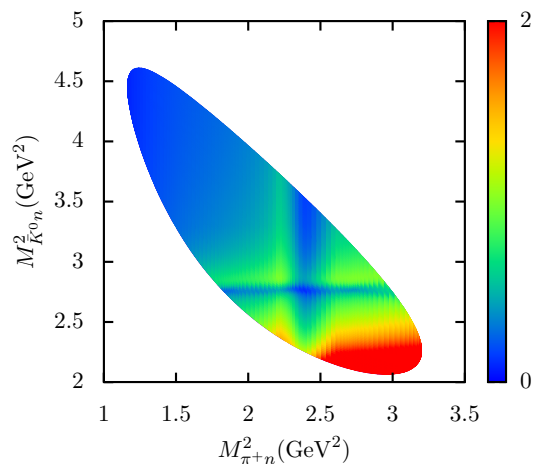


FIG. 8. Dalitz plot for the process  $\Lambda_c^+ \rightarrow n\bar{K}^0\pi^+$ .

peak appears around 1500 MeV, stemming directly from the  $N(1535)$  resonance. The  $\Lambda(1670)$  contribution to this distribution is relatively small and smooth. The peak's position and shape are robust predictions, which can be tested in future experiments like BESIII, Belle II, or LHCb experiments.

In the  $\bar{K}^0 n$  distribution (Fig. 7(b)), the most striking feature is a distinct dip around 1670 MeV, which is a signature of the  $\Lambda(1670)$  resonance. The  $N(1535)$  contribution provides a smooth background in this spectrum. The dip structure predicted here is qualitatively consistent with the behavior of  $\Lambda(1670)$  observed in  $\bar{K}N$  elastic scattering. This consistency supports the interpretation of  $\Lambda(1670)$  as a state dynamically generated from coupled-channel interactions, whose observable line shape is highly process-dependent. In  $\Lambda_c^+$  decay, the production mechanism and the interference with other amplitudes (e.g., from  $N(1535)$  and non-resonant terms) can modify the depth and exact location of the dip, but the underlying mechanism producing the dip remains the same.

Our findings suggest that the  $\Lambda(1670)$  contribution, which interferes with other isospin components, could play a key role in explaining the different effective isospin decompositions reported by BESIII and LHCb/Belle. A combined amplitude analysis of  $\Lambda_c^+ \rightarrow p\bar{K}^-\pi^+$  and  $\Lambda_c^+ \rightarrow n\bar{K}_S^0\pi^+$ , by taking into account these dynamically generated resonant contributions, would be crucial to resolve the apparent discrepancy, when the measurements of the process  $\Lambda_c^+ \rightarrow n\bar{K}^0\pi^+$  are available.

The Dalitz plot for  $\Lambda_c^+ \rightarrow \bar{K}^0\pi^+n$  in the plane of  $M_{\pi^+n}^2$  vs.  $M_{\bar{K}^0n}^2$  is shown in Fig. 8. A clear vertical band around  $M_{\pi^+n}^2 \approx 2.35 \text{ GeV}^2$  corresponding to the  $N(1535)$  signal and a horizontal band around  $M_{\bar{K}^0n}^2 \approx 2.79 \text{ GeV}^2$  ( $M_{\bar{K}^0n} \approx 1670 \text{ MeV}$ ) reflecting the  $\Lambda(1670)$  dip structure, appears as a region of reduced event density. This plot provides a comprehensive visualization of how the two resonances populate the decay phase space.

### C. Effects of Relative Phase and Color Factor

The coherent sum in Eq. (21) involves an unknown relative phase  $\phi$  between the two production mechanisms. Figure 9 shows the  $\pi^+n$  and  $\bar{K}^0n$  distributions for different values of  $\phi$ . The  $N(1535)$  peak in the  $\pi^+n$  spectrum can be significantly enhanced or suppressed, due to interference with the  $\Lambda(1670)$  amplitude. However, the position of the structure remains anchored near 1500 MeV. In the  $\bar{K}^0n$  spectrum, the  $\Lambda(1670)$  dip remains a robust feature for all phase values, although its depth and the surrounding background vary. Future precise data could potentially constrain this phase.

We also investigate the sensitivity to the color factor  $C$ , which parametrizes the relative weight of the external emission diagram. Figure 10 shows that the variation of  $C$  between 1.5 and 3 would change the overall normalization and the relative strength of the two resonant contributions, but does not qualitatively alter the peak and dip structures. The  $N(1535)$  peak and the  $\Lambda(1670)$  dip remain clearly identifiable.

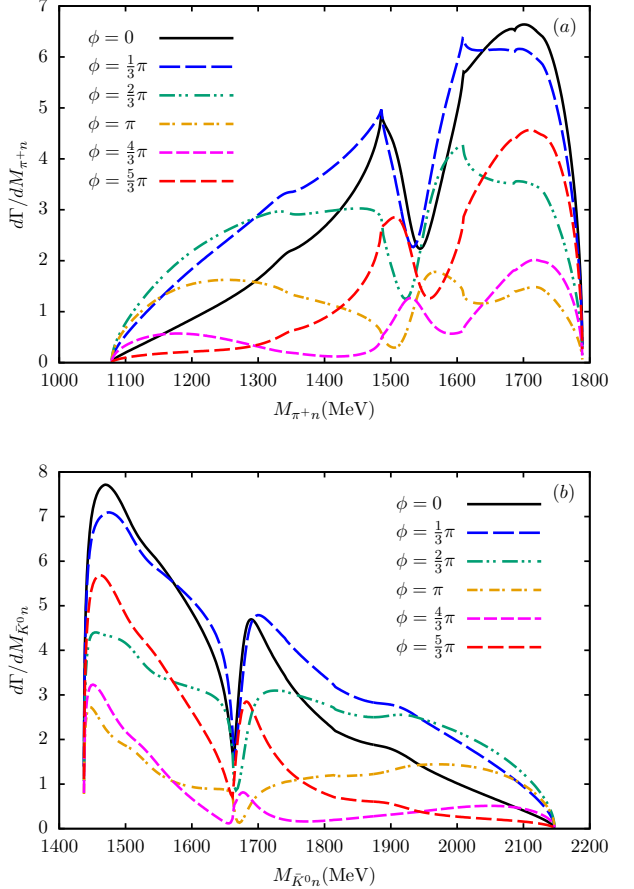


FIG. 9.  $\pi^+n$  (a) and  $\bar{K}^0n$  (b) invariant mass distributions of the process  $\Lambda_c^+ \rightarrow n\bar{K}^0\pi^+$  with the relative phase angle  $\phi = 0, \pi/3, 2\pi/3, \pi, 4\pi/3$ , and  $5\pi/3$ , respectively.

## IV. SUMMARY

In this work, we have presented a theoretical study of the Cabibbo-favored decay  $\Lambda_c^+ \rightarrow n\bar{K}^0\pi^+$  within the chiral unitary approach, where the low-lying resonances  $N(1535)$  and  $\Lambda(1670)$  are dynamically generated from the coupled-channel interactions. The investigation is motivated by recent experimental observations: a large branching fraction for  $\Lambda_c^+ \rightarrow n\bar{K}_S^0\pi^+$  that surpasses SU(3) predictions, and an apparent tension between the isospin decompositions of the  $\bar{K}N$  system reported by different experiments.

Our calculations predict a clear narrow peak in the  $\pi^+n$  invariant mass distribution, associated with the  $N(1535)$  resonance, and a distinct dip in the  $\bar{K}^0n$  distribution, associated with the  $\Lambda(1670)$  resonance. The dip structure is qualitatively consistent with the known behavior of  $\Lambda(1670)$  in  $\bar{K}N$  scattering, supporting its interpretation as a dynamically generated state. The significant contributions of these resonances can naturally explain the enhanced branching fraction and may play a crucial role in reconciling the different experimental findings regarding the  $\bar{K}N$  isospin composition.

The decay  $\Lambda_c^+ \rightarrow n\bar{K}^0\pi^+$  thus emerges as a powerful

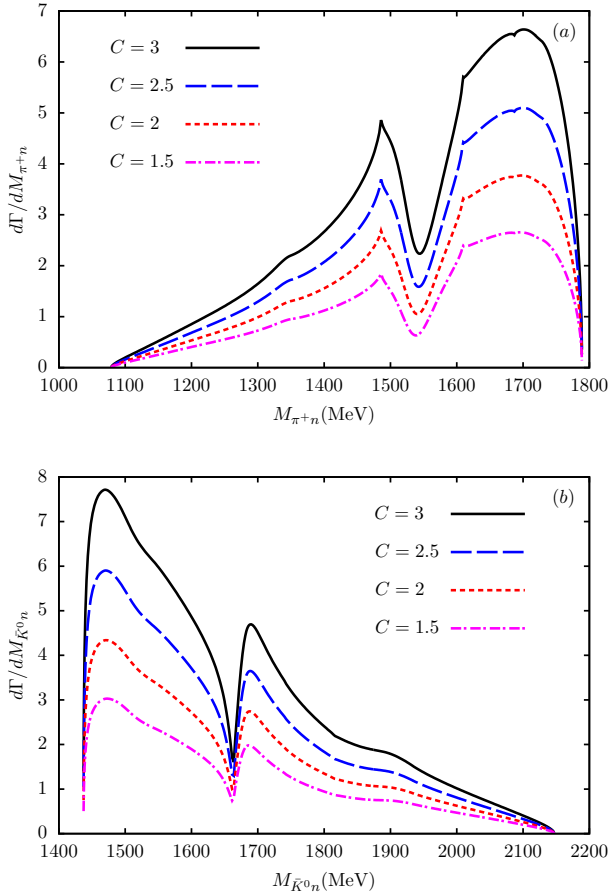


FIG. 10.  $\pi^+ n$  (a) and  $\bar{K}^0 n$  (b) invariant mass distributions of the process  $\Lambda_c^+ \rightarrow n\bar{K}^0\pi^+$  with the color factor  $C = 3, 2.5, 2$ , and  $1.5$ , respectively.

process to probe the nature of two contentious low-lying baryon resonances: the  $N(1535)$ , whose internal structure (three-quark, pentaquark, or molecular) is debated, and the  $\Lambda(1670)$ , which exhibits fascinating process-dependent line shapes. The predicted distributions and Dalitz plot can be used to test our model.

The absolute branching fraction of  $\Lambda_c^+ \rightarrow n\bar{K}^0\pi^+$  has been measured to be at the percent level. We strongly encourage high-statistics studies of this decay channel by the BESIII, Belle II, LHCb, and the proposed Super Tau-Charm Factory collaborations. Precise measurements of the  $\pi^+ n$  and  $\bar{K}^0 n$  invariant mass spectra, along with a full amplitude analysis, will be essential to confirm our predictions, constrain model parameters (like the relative phase  $\phi$  and the  $\Lambda(1670)$  subtraction constants), and ultimately shed light on the isospin dynamics and the internal structure of the  $N(1535)$  and  $\Lambda(1670)$  resonances.

## ACKNOWLEDGMENTS

This work is supported by the National Key R&D Program of China (No. 2024YFE0105200), the Natural Science Foundation of Henan under Grant No. 232300421140, the National Natural Science Foundation of China under Grant Nos. 12475086, 12192263, 12305137 and 12205075.

---

[1] M. Ablikim *et al.* [BESIII], Phys. Rev. D **112** (2025), 032006 doi:10.1103/csfn-p3h6 [arXiv:2506.02969 [hep-ex]].

[2] I. Adachi *et al.* [Belle and Belle-II], Phys. Rev. D **112** (2025) no.1, 012013 doi:10.1103/4mnw-tvks [arXiv:2503.04371 [hep-ex]].

[3] E. Wang, L. S. Geng, J. J. Wu, J. J. Xie and B. S. Zou, Chin. Phys. Lett. **41** (2024) no.10, 101401 doi:10.1088/0256-307X/41/10/101401 [arXiv:2406.07839 [hep-ph]].

[4] X. C. Feng, L. L. Wei, M. Y. Duan, E. Wang and D. M. Li, Phys. Lett. B **846** (2023), 138185 doi:10.1016/j.physletb.2023.138185 [arXiv:2009.08600 [hep-ph]].

[5] C. H. Zeng, J. X. Lu, E. Wang, J. J. Xie and L. S. Geng, Phys. Rev. D **102** (2020) no.7, 076009 doi:10.1103/PhysRevD.102.076009 [arXiv:2006.15547 [hep-ph]].

[6] Z. Wang, Y. Y. Wang, E. Wang, D. M. Li and J. J. Xie, Eur. Phys. J. C **80** (2020) no.9, 842 doi:10.1140/epjc/s10052-020-8347-2 [arXiv:2004.01438 [hep-ph]].

[7] M. Ablikim *et al.* [BESIII], Phys. Rev. Lett. **118** (2017) no.11, 112001 doi:10.1103/PhysRevLett.118.112001 [arXiv:1611.02797 [hep-ex]].

[8] M. Ablikim *et al.* [BESIII], Phys. Rev. D **109** (2024) no.7, 072010 doi:10.1103/PhysRevD.109.072010 [arXiv:2311.17131 [hep-ex]].

[9] C. Q. Geng, Y. K. Hsiao, C. W. Liu and T. H. Tsai, Phys. Rev. D **99** (2019) no.7, 073003 doi:10.1103/PhysRevD.99.073003 [arXiv:1810.01079 [hep-ph]].

[10] J. Y. Cen, C. Q. Geng, C. W. Liu and T. H. Tsai, Eur. Phys. J. C **79** (2019) no.11, 946 doi:10.1140/epjc/s10052-019-7467-z [arXiv:1906.01848 [hep-ph]].

[11] R. Aaij *et al.* [LHCb], Phys. Rev. D **108** (2023) no.1, 012023 doi:10.1103/PhysRevD.108.012023 [arXiv:2208.03262 [hep-ex]].

[12] S. B. Yang *et al.* [Belle], Phys. Rev. D **108** (2023) no.3, L031104 doi:10.1103/PhysRevD.108.L031104 [arXiv:2209.00050 [hep-ex]].

[13] S. C. Zhang, M. Y. Duan, W. T. Lyu, G. Y. Wang, J. Y. Zhu and E. Wang, Eur. Phys. J. C **84** (2024) no.12, 1253 doi:10.1140/epjc/s10052-024-13616-6 [arXiv:2405.14235 [hep-ph]].

[14] M. Y. Duan, M. Bayar and E. Oset, Phys. Lett. B **857** (2024), 139003 doi:10.1016/j.physletb.2024.139003 [arXiv:2407.01410 [hep-ph]].

[15] C. D. Lü, W. Wang and F. S. Yu, Phys. Rev. D **93** (2016) no.5, 056008 doi:10.1103/PhysRevD.93.056008 [arXiv:1601.04241 [hep-ph]].

[16] B. C. Liu and B. S. Zou, Phys. Rev. Lett. **96** (2006) no.4, 042002 doi:10.1103/PhysRevLett.96.042002 [arXiv:nucl-th/0503069 [nucl-th]].

[17] L. S. Geng, E. Oset, B. S. Zou and M. Doring, Phys. Rev. C **79** (2009), 025203 doi:10.1103/PhysRevC.79.025203 [arXiv:0807.2913 [hep-ph]].

[18] L. Hannelius and D. O. Riska, Phys. Rev. C **62** (2000), 045204 doi:10.1103/PhysRevC.62.045204 [arXiv:hep-ph/0001325 [hep-ph]].

[19] C. Helminen and D. O. Riska, Nucl. Phys. A **699** (2002), 624-648 doi:10.1016/S0375-9474(01)01294-5 [arXiv:nucl-th/0011071 [nucl-th]].

[20] A. Zhang, Y. R. Liu, P. Z. Huang, W. Z. Deng, X. L. Chen and S. L. Zhu, HEPNP **29** (2005), 250

[21] B. S. Zou, Eur. Phys. J. A **35** (2008), 325-328 doi:10.1140/epja/i2007-10561-8 [arXiv:0711.4860 [nucl-th]].

[22] E. Oset and A. Ramos, Nucl. Phys. A **635** (1998), 99-120 doi:10.1016/S0375-9474(98)00170-5 [arXiv:nucl-th/9711022 [nucl-th]].

[23] D. Jido, J. A. Oller, E. Oset, A. Ramos and U. G. Meissner, Nucl. Phys. A **725** (2003), 181-200 doi:10.1016/S0375-9474(03)01598-7 [arXiv:nucl-th/0303062 [nucl-th]].

[24] N. Kaiser, T. Waas and W. Weise, Nucl. Phys. A **612** (1997), 297-320 doi:10.1016/S0375-9474(96)00321-1 [arXiv:hep-ph/9607459 [hep-ph]].

[25] J. Nieves and E. Ruiz Arriola, Phys. Rev. D **64** (2001), 116008 doi:10.1103/PhysRevD.64.116008 [arXiv:hep-ph/0104307 [hep-ph]].

[26] T. Inoue, E. Oset and M. J. Vicente Vacas, Phys. Rev. C **65** (2002), 035204 doi:10.1103/PhysRevC.65.035204 [arXiv:hep-ph/0110333 [hep-ph]].

[27] M. Doring, E. Oset and B. S. Zou, Phys. Rev. C **78** (2008), 025207 doi:10.1103/PhysRevC.78.025207 [arXiv:0805.1799 [nucl-th]].

[28] E. Wang, H. X. Chen, L. S. Geng, D. M. Li and E. Oset, Phys. Rev. D **93** (2016) no.9, 094001 doi:10.1103/PhysRevD.93.094001 [arXiv:1512.01959 [hep-ph]].

[29] J. X. Lu, E. Wang, J. J. Xie, L. S. Geng and E. Oset, Phys. Rev. D **93** (2016), 094009 doi:10.1103/PhysRevD.93.094009 [arXiv:1601.00075 [hep-ph]].

[30] J. J. Xie and L. S. Geng, Phys. Rev. D **96** (2017) no.5, 054009 doi:10.1103/PhysRevD.96.054009 [arXiv:1704.05714 [hep-ph]].

[31] R. Pavao, S. Sakai and E. Oset, Phys. Rev. C **98** (2018) no.1, 015201 doi:10.1103/PhysRevC.98.015201 [arXiv:1802.07882 [nucl-th]].

[32] W. T. Lyu, Y. H. Lyu, M. Y. Duan, G. Y. Wang, D. Y. Chen and E. Wang, Eur. Phys. J. C **85** (2025) no.2, 123 doi:10.1140/epjc/s10052-025-13805-x [arXiv:2310.11139 [hep-ph]].

[33] Y. Li, S. W. Liu, E. Wang, D. M. Li, L. S. Geng and J. J. Xie, Phys. Rev. D **110** (2024) no.7, 074010 doi:10.1103/PhysRevD.110.074010 [arXiv:2406.01209 [hep-ph]].

[34] M. Y. Li, W. T. Lyu, L. J. Liu and E. Wang, Phys. Rev. D **111** (2025) no.3, 034046 doi:10.1103/PhysRevD.111.034046 [arXiv:2501.02859 [hep-ph]].

[35] J. Song, M. Bayar, Y. Y. Li and E. Oset, Eur. Phys. J. C **85** (2025) no.10, 1114 doi:10.1140/epjc/s10052-025-14870-y [arXiv:2507.19240 [hep-ph]].

[36] Y. Li, E. Wang, L. S. Geng and J. J. Xie, [arXiv:2601.13668 [hep-ph]].

[37] Z. W. Liu, W. Kamleh, D. B. Leinweber, F. M. Stokes, A. W. Thomas and J. J. Wu, Phys. Rev. Lett. **116** (2016) no.8, 082004 doi:10.1103/PhysRevLett.116.082004 [arXiv:1512.00140 [hep-lat]].

[38] D. Guo and Z. W. Liu, Phys. Rev. D **105** (2022) no.11, 114039 doi:10.1103/PhysRevD.105.114039 [arXiv:2201.11555 [hep-ph]].

[39] C. D. Abell, D. B. Leinweber, Z. W. Liu, A. W. Thomas and J. J. Wu, Phys. Rev. D **108** (2023) no.9, 094519 doi:10.1103/PhysRevD.108.094519 [arXiv:2306.00337 [hep-lat]].

[40] R. Molina, C. W. Xiao, W. H. Liang and E. Oset, Phys. Rev. D **109** (2024) no.5, 054002 doi:10.1103/PhysRevD.109.054002 [arXiv:2310.12593 [hep-ph]].

[41] H. P. Li, J. Song, W. H. Liang, R. Molina and E. Oset, Eur. Phys. J. C **84** (2024) no.7, 656 doi:10.1140/epjc/s10052-024-13015-x [arXiv:2311.14365 [hep-ph]].

[42] J. Y. Lee *et al.* [Belle], Phys. Rev. D **103** (2021) no.5, 052005 doi:10.1103/PhysRevD.103.052005 [arXiv:2008.11575 [hep-ex]].

[43] G. P. Gopal *et al.* [Rutherford-London], Nucl. Phys. B **119** (1977), 362-400 doi:10.1016/0550-3213(77)90002-5

[44] E. Oset, A. Ramos and C. Bennhold, Phys. Lett. B **527** (2002), 99-105 [erratum: Phys. Lett. B **530** (2002), 260-260] doi:10.1016/S0370-2693(01)01523-4 [arXiv:nucl-th/0109006 [nucl-th]].

[45] A. Starostin *et al.* [Crystal Ball], Phys. Rev. C **64** (2001), 055205 doi:10.1103/PhysRevC.64.055205

[46] X. H. Zhong and Q. Zhao, Phys. Rev. C **79** (2009), 045202 doi:10.1103/PhysRevC.79.045202 [arXiv:0811.4212 [nucl-th]].

[47] J. J. Liu, Z. W. Liu, K. Chen, D. Guo, D. B. Leinweber, X. Liu and A. W. Thomas, Phys. Rev. D **109** (2024) no.5, 054025 doi:10.1103/PhysRevD.109.054025 [arXiv:2312.13072 [hep-ph]].

[48] J. J. Xie and L. S. Geng, Eur. Phys. J. C **76** (2016) no.9, 496 doi:10.1140/epjc/s10052-016-4342-z [arXiv:1604.02756 [nucl-th]].

[49] G. Y. Wang, N. C. Wei, H. M. Yang, E. Wang, L. S. Geng and J. J. Xie, Phys. Rev. D **106** (2022) no.5, 056001 doi:10.1103/PhysRevD.106.056001 [arXiv:2206.01425 [hep-ph]].

[50] K. Miyahara, T. Hyodo and E. Oset, Phys. Rev. C **92** (2015) no.5, 055204 doi:10.1103/PhysRevC.92.055204 [arXiv:1508.04882 [nucl-th]].

[51] M. Y. Duan, W. T. Lyu, C. W. Xiao, E. Wang, J. J. Xie, D. Y. Chen and E. Oset, Phys. Rev. D **111** (2025) no.1, 016004 doi:10.1103/PhysRevD.111.016004 [arXiv:2410.16078 [hep-ph]].

[52] W. T. Lyu, S. C. Zhang, G. Y. Wang, J. J. Wu, E. Wang, L. S. Geng and J. J. Xie, Phys. Rev. D **110** (2024) no.5, 054020 doi:10.1103/PhysRevD.110.054020 [arXiv:2405.09226 [hep-ph]].

[53] Z. Y. Wang, S. Q. Luo, Z. F. Sun, C. W. Xiao and X. Liu, Phys. Rev. D **106** (2022) no.9, 096026 doi:10.1103/PhysRevD.106.096026 [arXiv:2211.08946 [hep-ph]].

[54] Y. Li, W. T. Lyu, G. Y. Wang, L. Li, W. C. Yan and E. Wang, Phys. Rev. D **111** (2025) no.5, 054011 doi:10.1103/PhysRevD.111.054011 [arXiv:2501.14385 [hep-ph]].

- [55] S. C. Zhang, W. T. Lyu, G. Y. Wang, B. Q. Ma and E. Wang, [arXiv:2601.12778 [hep-ph]].
- [56] K. Miyahara, T. Hyodo, M. Oka, J. Nieves and E. Oset, Phys. Rev. C **95** (2017) no.3, 035212 doi:10.1103/PhysRevC.95.035212 [arXiv:1609.00895 [nucl-th]].
- [57] R. P. Pavao, W. H. Liang, J. Nieves and E. Oset, Eur. Phys. J. C **77** (2017) no.4, 265 doi:10.1140/epjc/s10052-017-4836-3 [arXiv:1701.06914 [hep-ph]].
- [58] A. Bramon, A. Grau and G. Pancheri, Phys. Lett. B **283** (1992), 416-420 doi:10.1016/0370-2693(92)90041-2
- [59] E. Oset, W. H. Liang, M. Bayar, J. J. Xie, L. R. Dai, M. Albaladejo, M. Nielsen, T. Sekihara, F. Navarra and L. Roca, *et al.* Int. J. Mod. Phys. E **25** (2016), 1630001 doi:10.1142/S0218301316300010 [arXiv:1601.03972 [hep-ph]].
- [60] M. Doring, E. Oset and D. Strottman, Phys. Rev. C **73** (2006), 045209 doi:10.1103/PhysRevC.73.045209 [arXiv:nucl-th/0510015 [nucl-th]].
- [61] S. Navas *et al.* [Particle Data Group], Phys. Rev. D **110** (2024) no.3, 030001 doi:10.1103/PhysRevD.110.030001